Acta Cryst. (1989). A**45**, 428-431

Effects of a Stacking Fault on Higher-Order Diffraction Fringes*

BY RENHUI WANG AND JIANGUO WEN

Department of Physics, Wuhan University, 430072 Wuhan, People's Republic of China and Beijing Laboratory of Electron Microscopy, Academia Sinica, PO Box 2724, 100080 Beijing, People's Republic of China

(*Received 7 November 1988; accepted 18 January 1989*)

Abstract

The effect of the depth z_0 of a stacking fault and the specimen thickness t on the displacement and splitting of higher-order diffraction fringes has been observed experimentally by means of large-angle convergent-beam electron diffraction and simulated theoretically under the two-beam dynamical approximation. Moreover, a quantitative relationship between the displacement and splitting of a diffraction fringe on the one hand and the displacement vector **R** of the stacking fault, the specimen thickness t, and the diffraction-vector amplitude g on the other hand, was deduced in the thin-specimen approximation when the fault lies at the midpoint of the specimen ($z_0 = t/2$).

1. Introduction

Carpenter & Spence (1982) first studied the splitting of higher-order Laue-zone (HOLZ) lines when the convergent-beam electron diffraction (CBED) probe was positioned approximately over an isolated straight dislocation. Fung (1985) studied the displacement and splitting of diffraction fringes in CBED patterns caused by transverse stacking faults in graphite and dislocations in silicon. Tanaka & Kaneyama (1986) and Tanaka, Terauchi & Kaneyama (1988) studied intensity profiles of both lower- and higher-order reflections using the large-angle CBED (LACBED) technique and two-beam approximation. The results show that diffraction fringes with $\alpha = 2\pi n$ (n = integer) are not affected by stacking faults whereas those with $\alpha = 2\pi/3$ ($\alpha = -2\pi/3$) do split into several peaks of which the strongest peak lies at the position with $w < 0$ ($w > 0$). Wen, Wang & Fung (1987) calculated theoretical rocking curves for the $\pm 10\bar{1}0$ and $\pm 20\bar{2}0$ reflections of graphite containing a stacking fault using the two-beam dynamical approximation and arrived at a good agreement with Fung's experimental results. Recently, Chou, Zhao & Ko (1989) studied HOLZ-line effects of a stacking fault in a stainless steel both experimentally and theoretically.

Higher-order reflections possess greater extinction distances ξ_g and hence satisfy the so-called 'thin specimen approximation'. In addition, a stacking fault is the simplest defect for theoretical treatment. As the first step for the theoretical study of the effect of the defect on the displacement and splitting of diffraction fringes, we rearranged the analytical expressions for the transmitted intensity of a crystal containing a stacking fault in the two-beam case. Then a simple quantitative relationship between the displacement and splitting of a diffraction fringe on the one hand and the displacement vector **R** of the stacking fault, the diffraction vector **g**, its modulus g, and the specimen thickness t on the other hand, when the stacking fault lies at the midpoint of the specimen, was deduced under the thin-specimen approximation suitable for higher-order reflections. Moreover, in this work we observed experimentally the dependence of the displacement and splitting of higher-order reflections on the fault depth z_0 and the specimen thickness t using LACBED. There is good agreement between these observations and the theoretical calculations in this work.

2. Experimental results

1Cr18Ni9Ti austenitic stainless steel plates were thinned chemically in a solution of HNO_3:HCl = 1:3 to a thickness of nearly 0·1 mm. From these plates transmission electron microscopy (TEM) specimens were prepared by means of twin-jet polishing in a solution of $HClO_4$:C_2H_5OH = 1:9. LACBED studies were carried out in a Philips EM 420 electron microscope.

Figs. 1(*a*), (*b*) and (*c*) show [114] zone-axis Tanaka patterns at 100 kV of the austenitic stainless steel specimen containing a stacking fault oblique to the specimen surface. The horizontal grey ribbons marked SF are shadow images of the stacking fault which intersects different areas of the [114] Tanaka pattern in these three figures. Fig. 1(*d*) shows a simulated [114] zone-axis HOLZ line pattern of a perfect stainless steel, which possesses a vertical mirror line. Such mirror symmetry is lost in (*a*), (*b*) and (*c*) where the intersecting point of the $\bar{9}\bar{1}3$ and $\bar{1}\bar{9}3$ lines is shifted to the right-hand side of the mirror line. From

* Project supported by the National Natural Science Foundation of China.

0108-7673/89/060428-04$03.00

the conventional trace analysis the displacement vector **R** of this stacking fault was determined to be $\frac{1}{3}[111]$ and the specimen thickness t has a mean value of about 70 nm.

When crossing the shadow image of the stacking fault, each HOLZ line becomes wider, then splits into two lines whose separation increases and arrives at a maximum at the midpoint of the shadow image of the stacking fault. This widening and splitting behaviour is symmetrical about the midpoint of the shadow image. Such behaviour corresponds exactly to the dependence of the widening and splitting of HOLZ lines on the fault depth z_0.

The widths of the shadow images in Figs. 1 (a), (b) and (c) decrease from the left-hand side to the right-hand side, which means a decrease of the specimen thickness t. In (a), the separation of the split $\bar{3}9\bar{1}$ line is greater than that of the $9\bar{3}\bar{1}$ line, whereas the separation of the split $\bar{3}9\bar{1}$ line is smaller than that of the $9\bar{3}\bar{1}$ line in (c). This means that the separation of a split HOLZ line caused by a stacking fault increases with a decrease of the specimen thickness t.

3. Theoretical calculations

Describing the influence of crystal defects on the diffraction intensity by three parameters q, α_p and α_q, we can write the transmitted intensity I_T as (Katerbau, 1981; Wen, Wang & Fung 1987)

$$I_T = \exp(-2\pi t/\xi_0')(T_1 + T_2 + T_3) \tag{1}$$

with

$$T_1 = \frac{1-q^2}{1+w^2}\left\{1+\sinh^2\left[\frac{\pi(t+2t_w)}{\xi_g'(1+w^2)^{1/2}}\right] - \sin^2\left[\frac{\pi t(1+w^2)^{1/2}}{\xi_g}+\alpha_p\right]\right\} \tag{2}$$

$$T_2 = \frac{q^2}{1+w^2}\left\{\sinh^2\left(\frac{\pi(t-2z_0)}{\xi_g'(1+w^2)^{1/2}}\right) + \sin^2\left[\frac{\pi(t-2z_0)(1+w^2)^{1/2}}{\xi_g}-\alpha_g\right]\right\} \tag{3}$$

$$T_3 = \frac{q(1-q^2)^{1/2}}{1+w^2}\left\{\sinh\left(\frac{2\pi(t_w+z_0)}{\xi_g'(1+w^2)^{1/2}}\right) \times\cos\left[\frac{2\pi(t-z_0)(1+w^2)^{1/2}}{\xi_g}+\alpha_p-\alpha_g\right] - \sinh\left[\frac{2\pi(t_w+t-z_0)}{\xi_g'(1+w^2)^{1/2}}\right] \times\cos\left[\frac{2\pi z_0(1+w^2)^{1/2}}{\xi_g}+\alpha_p+\alpha_q\right]\right\} \tag{4}$$

where ξ_0' denotes the mean absorption length, ξ_g' the anomalous absorption length, $w = s\xi_g$ the dimensionless deviation parameter with $s = g\Delta\theta$ and $\Delta\theta$ being the deviation from the Bragg condition for the reciprocal vector **g**. w is replaced in some cases by a characteristic thickness t_w given by

$$w = \sinh[2\pi t_w/\xi_g'(1+w^2)^{1/2}]. \tag{5}$$

For the case of a single stacking fault with a displacement vector **R** we have

$$q = |\sin(\alpha/2)|/(1+w^2)^{1/2} \tag{6}$$

$$\alpha_p = \tan^{-1}\{[w/(1+w^2)^{1/2}]\tan(\alpha/2)\} \tag{7}$$

and

$$\alpha_q = m\pi/2 \tag{8}$$

with

$$\alpha = 2\pi\mathbf{g}\,.\,\mathbf{R}$$

$$m = \sin(\alpha/2)/|\sin(\alpha/2)|.$$

From the expressions described above it is concluded that (1)-(4) reduce to the expressions for a perfect crystal when $\alpha = 2\pi n$ (n = integer), which agrees with Fung's observation. Another conclusion is that the transmitted rocking curves for the fault depths z_0 and $t - z_0$ are the same. This conclusion is in good agreement with the observed symmetry of the behaviour of the displacement and splitting of a HOLZ line about the midpoint of the specimen. In

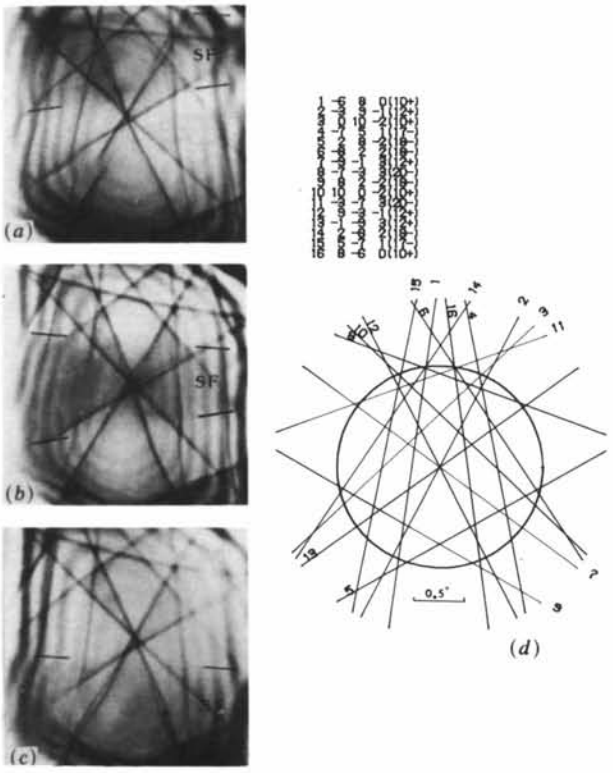

Fig. 1. [114] zone-axis Tanaka patterns at 100 kV of an austenitic stainless steel containing a stacking fault. (a), (b), (c) Experimental patterns with shadow images of the stacking fault (marked SF). (d) Simulated HOLZ-line pattern.

the following some results for stainless steel calculated from expressions mentioned above are reported.

Fig. 2 shows the transmitted intensity I_T as a function of the deviation angle $\Delta\theta$ from the Bragg condition for different specimen thicknesses t when the stacking fault lies at the midpoint of the TEM specimen ($z_0 = t/2$) and $\mathbf{g} = \bar{3}9\bar{1}$, $\mathbf{R} = [111]/3$, $\xi_g = 310$ nm (at 100 kV) and $\xi_g/\xi'_g = 0{\cdot}05$. Fig. 3 shows the transmitted intensity I_T as a function of $\Delta\theta$ for different higher-order reflections $\mathbf{g}$ when $z_0 = t/2 = 50$ nm, $\mathbf{R} = [111]/3$, $\xi_g/\xi'_g = 0{\cdot}10$, and $\xi_g = 183$, 340 and 454 nm for the $\bar{1}17$, $\bar{6}80$ and $\bar{6},10,0$ reflections respectively. From similar calculations it is found that when $z_0 = t/2$ and $t \leq \xi_g/2$, each higher-order diffraction fringe is split into two fringes, one stronger (at $\Delta\theta_1$) and the other weaker (at $\Delta\theta_2$). These two peaks lie at opposite sides of the Bragg position ($\Delta\theta_1/\Delta\theta_2 < 0$). For the $\bar{1}17$ and $\bar{6},10,0$ reflections, $\alpha = 2\pi/3 > 0$, the stronger peak lies on the side with $\Delta\theta_1 < 0$, whereas for the $\bar{3}9\bar{1}$ and $\bar{6}80$ reflections we have $\alpha = -2\pi/3 < 0$ and the stronger peak on the side with $\Delta\theta_1 > 0$. The displacement amounts $\Delta\theta_1$ and $\Delta\theta_2$ of these two peaks and their separation $\Delta\theta = |\Delta\theta_1 - \Delta\theta_2|$ are all inversely proportional to the product of the specimen thickness t and the modulus g of the diffraction vector. These conclusions coincide with our experiment and the results obtained by Fung (1985), Tanaka & Kaneyama (1986) and Tanaka, Terauchi & Kaneyama (1988).

Fig. 4 shows the calculated variation of the displacement and splitting of the $\bar{3}9\bar{1}$ diffraction fringe with the fault depth z_0 when $t = 80$ nm, $\mathbf{R} = [111]/3$, $\xi_g = 310$ nm (at 100 kV) and $\xi_g/\xi'_g = 0{\cdot}05$. Owing to the symmetry property of the transmitted rocking curve about the midpoint of the specimen, we need only vary the value of z_0/t from 0 to 1/2. It is found from Fig. 4 and similar calculations for $t = 40$–200 nm

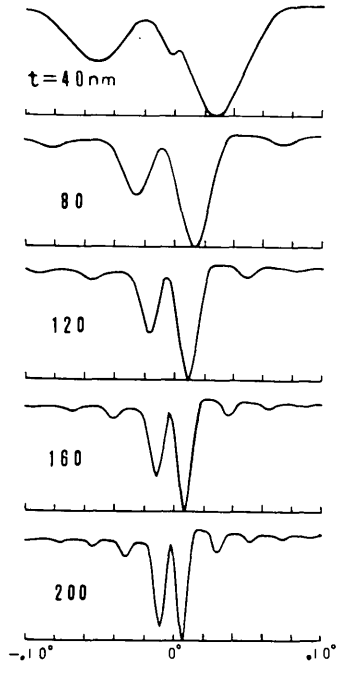

Fig. 2. Calculated transmitted intensity as a function of the deviation angle $\Delta\theta$ for different specimen thicknesses t when $z_0 = t/2$, $\mathbf{g} = \bar{3}9\bar{1}$, $\mathbf{R} = 1/3[111]$, $\xi_g = 310$ nm (at 100 kV) and $\xi_g/\xi'_g = 0{\cdot}05$.

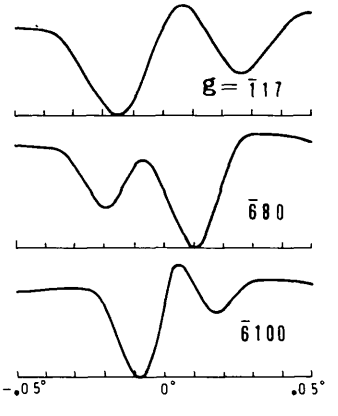

Fig. 3. Calculated transmitted intensity as a function of the deviation angle $\Delta\theta$ for different reflections $\mathbf{g}$ when $z_0 = t/2 = 50$ nm, $\mathbf{R} = [111]/3$, $\xi_g/\xi'_g = 0{\cdot}10$, and $\xi_g = 183$, 340 and 454 nm for the $\bar{1}17$, $\bar{6}80$ and $\bar{6},10,0$ reflections respectively.

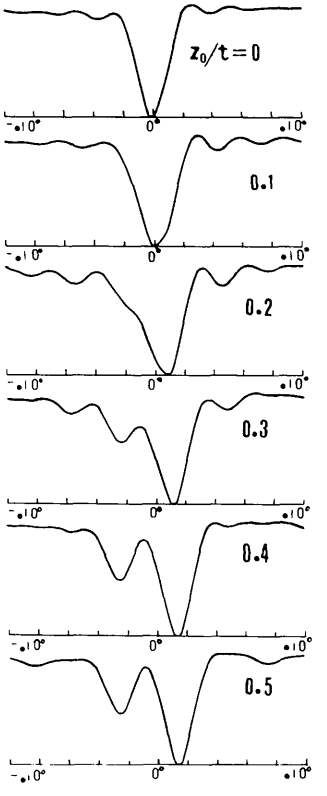

Fig. 4. Calculated variation of the displacement and splitting of the $\bar{3}9\bar{1}$ diffraction fringe with the fault depth z_0 when $t = 80$ nm, $\mathbf{R} = [111]/3$, $\xi_g = 310$ nm (at 100 kV), $\xi_g/\xi'_g = 0{\cdot}05$.

that the diffraction fringe is not affected by the stacking fault lying at the specimen surface ($z_0/t=0$) and appears as a dark peak (HOLZ line). This line becomes wider with the increase of fault depth z_0, begins to split at $z_0/t\simeq 1/4$ and arrives at maximum separation at $z_0/t=1/2$. The variation of calculated $\bar{3}9\bar{1}$ HOLZ-line positions expressed as $gt\Delta\theta_1$ and $gt\Delta\theta_2$ with z_0/t are shown schematically in Fig. 5 with $\mathbf{R}=[111]/3$, $t=100$ nm, $\xi_g=310$ nm (at 100 kV) and $\xi_g/\xi_g'=0{\cdot}10$. The agreement between Fig. 5 and HOLZ lines in Figs. 1(*a*), (*b*) and (*c*) is very good.

4. Thin-specimen approximation

For higher-order reflections the condition $t<\xi_g/2$ is usually fulfilled. When $|w|>1$, then $|t_w|\geq\xi_g'/5$, and hence $t\ll|t_w|$. Under these conditions the sinh terms in (2) and (4) can be replaced simply by w owing to (5). In this case, when $w^2\gg 1$ *and* $z_0/t\simeq 1/2$, expressions (1)-(4) are simplified to

$$I_T=1-(1/w^2)[\sin^2(\alpha/2)-2\sin(\alpha/2)\times\sin(\pi tg\Delta\theta+\alpha/2)+\sin^2(\pi tg\Delta\theta+\alpha/2)]. \quad (9)$$

From this expression it is found that, for $\alpha=\pm 2\pi/3$, the positions at which I_T reaches at a minimum value are determined mainly by $(1/w^2)\sin(\pi tg\Delta\theta+\alpha/2)$. The last term has only the effect of varying the minimum value. Therefore, the w, s or $\Delta\theta$ values at which I_T reaches a minimum are just the w, s or $\Delta\theta$ values at which $(1/w^2)\sin(\pi tg\Delta\theta+\alpha/2)$ reach extrema. These values are determined by the equation

$$\tan(\pi tg\Delta\theta+\alpha/2)=(1/2)\pi tg\Delta\theta. \quad (10)$$

For $\alpha=m2\pi/3$ the first two $\Delta\theta$ values corresponding to the first two split HOLZ lines are obtained numerically as

$$\Delta\theta_1(\text{rad})=-0{\cdot}564m/(gt) \quad (11)$$

$$\Delta\theta_2(\text{rad})=0{\cdot}984m/(gt). \quad (12)$$

They possess opposite signs and have a ratio

$$\Delta\theta_2/\Delta\theta_1=-1{\cdot}74 \quad (13)$$

and their separation is

$$\Delta\theta(\text{rad})=|\Delta\theta_1-\Delta\theta_2|=1{\cdot}548/gt. \quad (14)$$

Owing to the steep attenuation factor $1/w^2$ the peak which lies mostly adjacent to the Bragg position, *i.e.* the peak at $\Delta\theta_1$, has larger intensity than the next peak at $\Delta\theta_2$. Other peaks have too small intensity and may be omitted. All these conclusions are in good agreement both with the simulated results shown in Figs. 2 and 3 and the experimental observations shown in Figs. 1 (*a*), (*b*) and (*c*) of this paper, and obtained by Fung (1985), Tanaka & Kaneyama (1986), Chou, Zhao & Ko (1988) and Tanaka, Terauchi & Kaneyama (1988).

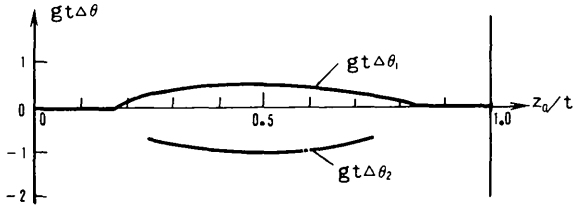

Fig. 5. Variation of simulated $\bar{3}9\bar{1}$ HOLZ-line positions expressed as $gt\Delta\theta_1$ and $gt\Delta\theta_2$ with z_0/t when $\mathbf{R}=[111]/3$, $t=100$ nm, $\xi_g=310$ nm (at 100 kV) and $\xi_g/\xi_g'=0{\cdot}10$.

References

CARPENTER, R. W. & SPENCE, J. C. H. (1982). *Acta Cryst.* A**38**, 55-61.

CHOU, C. T., ZHAO, L. T. & KO, T. (1989). In preparation.

FUNG, K. K. (1985). *Ultramicroscopy*, **17**, 81-86.

KATERBAU, K.-H. (1981). *Philos. Mag.* A**43**, 409-426.

TANAKA, M. & KANEYAMA, T. (1986). Proc XIth Int. Congr. Electron Microsc., Kyoto, Japan, 1986, pp. 203-206.

TANAKA, M., TERAUCHI, M. & KANEYAMA, T. (1988). *Convergent-Beam Electron Diffraction.* Tokyo: JEOL-Maruzen.

WEN, J., WANG, R. & FUNG, K. K. (1987). Proc. 4th Chin.-Jpn Electron Microsc. Seminar.